Research Article : Open Access

DOI: 10.35840/2631-5033/1869

VIBGYOR ePress

International Journal of
Earth Science and Geophysics

Integration of Geophysical Resistivity Inversion along with Hydrological Investigation in Scrutiny of El-Tour Coastal Aquifer

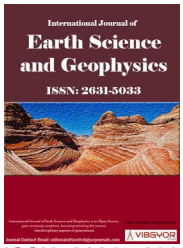

ISSN: 2631-5033

Noha A Hassan* and Mohamed H Khalil*

Geophysics Department, Faculty of Science, Cairo University, Giza, Egypt

Abstract

Groundwater constitutes the foremost source of freshwater in El-Tor city, South Sinai, Egypt. In this context, a hypothetical mechanism amalgamating one-dimension (1D) Schlumberger geoelectric resistivity inversion, geohydrological analysis, borehole data is conducted to define aquifer geometry states in the study area. Furthermore, pumping tests along with hydro-chemical analysis is employed in the area.

Qualitative and quantitative modelling of the inverted resistivity data efficiently delineated the fresh aquifer with true resistivity ranging between 71 to 110 Ohm.m, and thickness ranging between 55 to 90 m. Furthermore, aquifer loss in relation to the pumping regime was characterized as well. The eastern section of the freshwater aquifer characterized by thickness increase (90 m), tortuosity (1.31), hydraulic conductivity (63 m/day), transmissivity (5077 m2/day), formation resistivity factor (4.5), and storativity (0.224). Moreover, it characterized by decreased values of electrical conductivity (0.048~0.356 mS/m), electric anisotropy (1), mean resistivity (255 ohm.m), porosity (37%), and total dissolved solid (TDS) (496 ppm).

Keywords

Schlumberger resistivity, Electric and hydraulic parameters, TDS, Pumping regime

Introduction

Due to their strategic locations, coastal cities have been given significant attention throughout the decades. This attention has been outstandingly emulated in founding new settlements, tourism, industrial, cultivation, as well as mega-economic progressive projects. Thus, the demand of the freshwater in these cities considerably increased. Since Sinai Peninsula in general and El-Tor in particular are areas where no widespread aquifer damage has been manifested, a convenient groundwater quality protection program can be effective in preserving natural groundwater quality. On account of the absence of naturally occurring and/or recharged surface water, it is highly vital to particularly concern about the status of the groundwater. Of the most important interests is the quality and quantity of the groundwater, coupled with any natural or anthropogenic hazards, causing groundwater contamination. El-Tor is the administrative capital of South Sinai Governorate. Worth mentioning, the city was named after the Arabic name of the mountain in which the prophet Moses received the tablets from God. Furthermore, El-Tor is a rapidly developing city with a number of

***Corresponding author:** *Noha A Hassan, Geophysics Department, Faculty of Science, Cairo University, Giza, Egypt*

Accepted: June 06, 2023; **Published:** June 08, 2023

Citation: Hassan NA, Khalil MH (2023) Integration of Geophysical Resistivity Inversion along with Hydrological Investigation in Scrutiny of El-Tour Coastal Aquifer. Int J Earth Sci Geophys 9:069

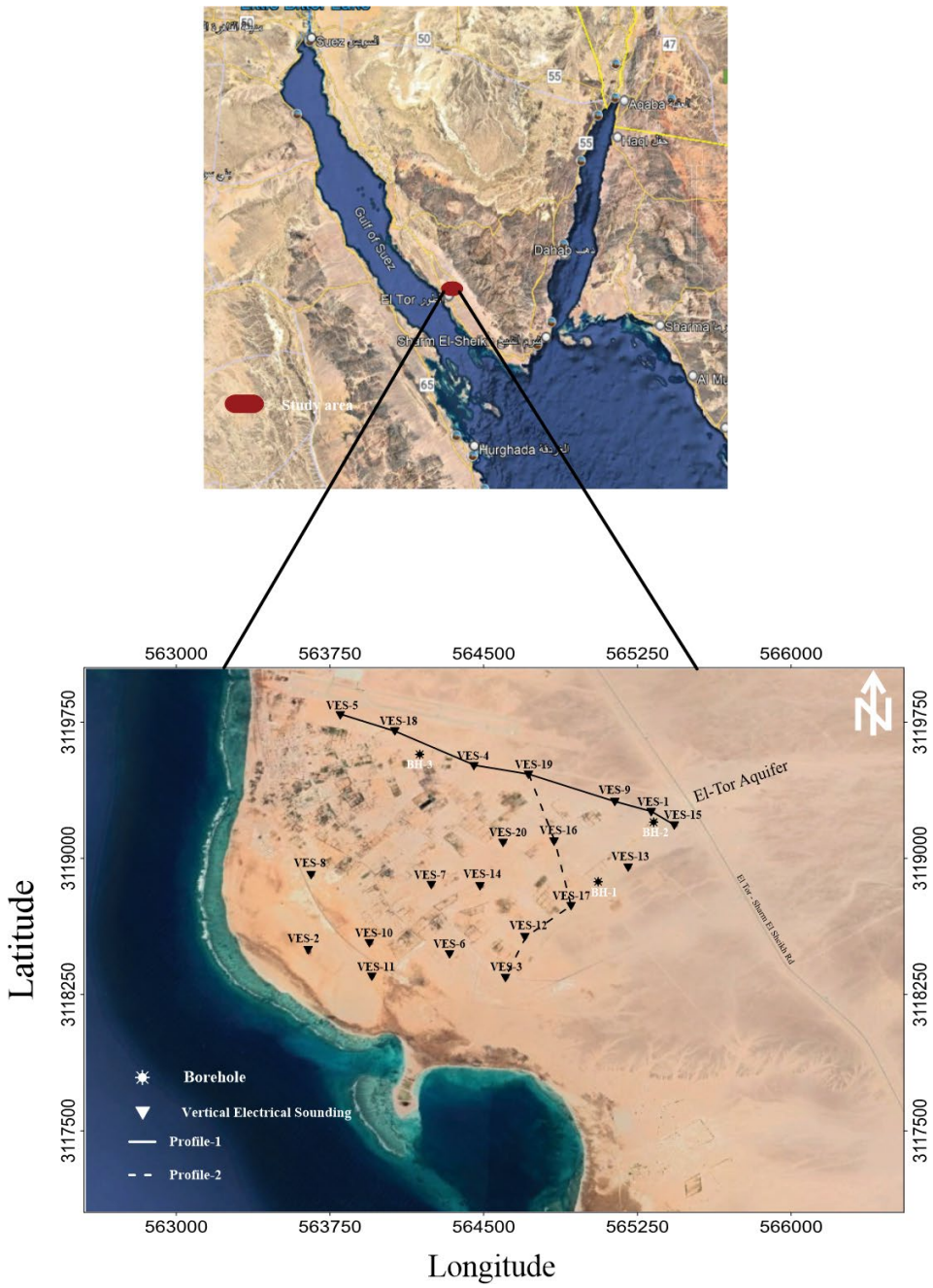

Figure 1: Location map of the study area, El-Tor, Gulf of Suez, South Sinai [2].

different tourist accommodations and amenities. The study area (El-Tor) is located in the middle sector of the El-Qaa plain, south-east Gulf of Suez, Sinai (Figure 1). The area is bounded by longitude and latitude 563000 to 566000 N and 3117500 to 3119750 E, respectively covering an area of about 4 by 3 km (12 km^2). Furthermore, the screened groundwater bores in the El-Qaa Quaternary alluvial aquifer yield up to 16,000 m^3/day. Although, the water is slightly brackish with total dissolved solids (TDS) of 500 ppm, it's mainly employed for drinking in El-Tor as well as Sharm El-Sheikh [1]. In this context, a number of electrical conditions, conjoined with aquifer hydraulic parameters were investigated for the freshwater aquifer in the study area. Moreover, the effect of the pumping regime (pumping rate, well loss, well specific capacity, and well efficiency) in aquifer loss was analyzed.

Geological and Structure Setting

As mentioned by Rushdi Saidin [3], Gulf of Suez is the north-western arm of the Red Sea rift system which is bounded by a major border extensional fault. Not only, the El-Qaa plain is a secondary rift

basin trending NNW-SSE parallel to the main rift system of the Gulf. But also, there is a conspicuous syncline plunging S-E in El Qaa plain northern zone. Sultan, et al. [4] established that the El-Qaa Quaternary alluvial aquifer is considered the main freshwater source in the El-Tor region. Moreover, the aquifer is characterized by the presence of Quaternary alluvial fans surrounded by igneous and metamorphic Pre-Cambrian rocks. Praiseworthy, there are about ten main wadis (dry ephemeral riverbed) dissevering the basement terrain and draining the water via the El-Qaa plain. The water quality data from El-Qaa aquifer designated that there is a distinct fresh/saline water transition zone across the aquifer upon which fresh surface water runs off from the wadis, recharges as well as mixes with saline groundwater [4-7]. Although seawater intrusion phenomenon is a very usual and is a widespread environmental problem in the El-Qaa plain, it has significant contribution to the salinity of the groundwater [4,8-11]. Noteworthy, saltwater intrusion may transpire due to human activities and/or by natural calamities such as climate change as well as sea level rise. The authority of the geological survey of Egypt, [12] elucidated the subsurface stratigraphy in the area through the drilled boreholes. According to the borehole description, El-Qaa is divided into three geomorphologic units, the eastern mountainous region, the western sedimentary hills, and the central plain [13,14]. The eastern mountainous district (Pre-Cambrian crystalline basement complex) is an allotment of the Arabian-Nubian shield discriminated by high relief ranging between 300 and 2662 m amsl. The eastern mountains are comprised of igneous and metamorphic rocks acting as a recharge boundary along the wadi outlets [15]. Notably, the western sedimentary hills encompass the Gebel Qabaliat ridge and embodied of different sedimentary units along with basement rocks. This unit has an average elevation of 250m amsl, with a moderate slope towards the El-Qaa plain. This unit is characterized by a dense consequent net of drainage lines. The central plain unit in which the study area is located is outlined as a peneplain developed and produced during the Quaternary period. It is distinguished by being dissected by wadi courses, terraces, playa deposits and alluvial fans in which both sand dunes and sheets are observed along with being flat [16]. Shata, et al. [5] emphasized the alluvial deposits of this unit by high-storage capacity and receive appreciable amounts of recharge from the surrounding eastern mountains. Significantly, the alluvial processes play a major role in the formation and evolution of the alluvial fans. The fans store water percolated and drained by the wadi's drainage net. Beyond that, the groundwater potential of this structural basin depends upon the features of the rock units and the recharge conditions. Based on the aridity view of El-Tor region along with El-Tor arid climate, almost all-present and future freshwater needs goanna have to be acquired from local groundwater aquifers [6]. Withal, direct rain over El-Qaa plain Quaternary aquifer is about 10 mm/y and reaches about 60 mm/y over the high surrounding basement rocks with heavy storms producing floods every few years. Although most of the precipitation occurs in wintertime, occasional torrential showers are expected in spring as well as in autumn and are associated with the monsoon winds coming from the south-east [17]. The water level of the Quaternary aquifer in El-Tor is fluctuating according to various annual recharging conditions with NE-SW flow direction [18]. Sultan, et al. [4], indicated that the aquifer discharges groundwater either to the coastal sabkha or to the Gulf of Suez. Conspicuously, numerous hydro-geophysical investigations have been conducted in the area bysundry authors [4,8-10,13,18-28]. The common subsurface section of the area aggregated from the available boreholes data is illustrated in Figure 2.

Methodology

Geoelectrical measurements

The methodology of Schlumberger geo-electrical resistivity sounding (VES) together with its implementation in groundwater investigation has been utilized by many authors [15,29-36]. According to Lashkarippour, et al. [37], the material's resistivity is influenced by numerous factors such as groundwater salinity, saturation, aquifer lithology, as well as porosity. Furthermore, the relevance between aquifer characteristics with the layer electrical parameters have been studied and reviewed by many authors [17,27,32,38-43].

1D Geoelectric data inversion

Considering that sediments resistivity is one of the most variable physical properties along with the interpretation vagueness, it became vital to correlate the observed VES data with the available borehole data. This correlation enables

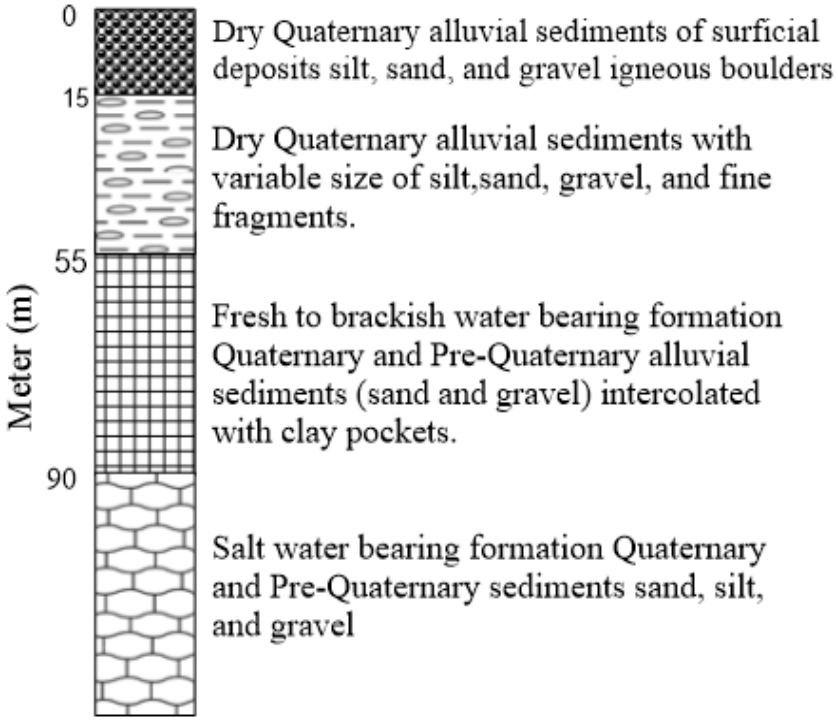

Figure 2: Generalized subsurface stratigraphic section in the study area.

assigning resistivity ranges to various lithologic units. On the other hand, the collected field data were interpreted through the following steps: (a) Matching the field curve with the standard curves of the auxiliary method [44,45], (b) Preparing a forward model consisting of a limited number of geo-electric layers founded on available borehole data (thicknesses and corresponding resistivities) [46], as well as (c) Entering the initial geo-electrical model into the IPI2 Win geo-electric modeling package [47,48].

Aquifer hydraulic conditions

A considerable number of investigation either measured or/and gauged were employed to identify a number of the significant freshwater aquifer hydraulic conditions in the study area. In this context, pumping tests together with a number of borehole samples analyses were conducted for BH-2 and BH-3. Two types of pumping tests were carried out, the first was a long-lasting pumping with a long duration at constant discharge, while the other is a step pumping test with variable discharge rates.

Aquifer electrical conditions

A. Electric anisotropy (λ)

The quantitative interpretation of the geo-electric sounding data is meaningful if a horizontally stratified layers characterized by a certain resistivity and thickness for each layer is present in conjunction with electric anisotropy [49-53]. Dar Zarrouk Parameters (DZ) were first introduced by Maillet [54], and it deals with the explanation and identification of electric anisotropy (λ) from the VES. Unless the column is completely uniform, Majumdar and Das, [55] implies that the average resistivity gauged for a current flow vertically through such a column will differ from that flowing horizontally. Not only has this dependence of resistivity on direction of current flow comprised an effective anisotropy, caused by the layering and not by the inherent anisotropy within the layers [56]. But also, it can be fundamentally attributed to the fact that the longitudinal resistivity (ρ_l) is less than the transverse resistivity (ρ_t), meaning that the current flow density along the bedding planes is greater than that normal to the bedding planes.

Dar Zarrouk parameters can be reckoned as follow;

Longitudinal unit conductance: $S_i = h_i/\rho_i$

The total longitudinal conductance:

$$S_t = \sum_{i=1}^{n} (h_i/\rho_i)$$

Longitudinal resistivity:

$$\rho_l = H/S = \sum_{i=1}^{n} h_i \Big/ \sum_{i=1}^{n} (h_i/\rho_i)$$

Transverse unit resistance: $T_t = h_i * \rho_i$

The total transverse resistance:

$$T_t = \sum_{i=1}^{n} (h_i * \rho_i)$$

Transverse resistivity:

$$\rho_t = T/H = \sum_{i=1}^{n} (h_i \quad \rho) \Big/ \sum_{i=1}^{n} h_i$$

Electric anisotropy: $\lambda = (\rho_t/\rho_l)^{1/2} > 1$

Root mean square resistivity:

$$\rho_m = (\rho_t * \rho_l)^{1/2} = \lambda * \rho_l = (1/\lambda) * \rho_t$$

Where; ρ_i is the true resistivity and h_i is the thickness for each layer (i).

B. Electric conductivity (EC)

Electrical conductivity (EC) stands for the measurement of the dissolved material in an aqueous solution coupled with the ability of the material to conduct electrical current through it. The higher the dissolved material in water or soil, the higher the EC will be in that material. Electrical conductivity (EC) can be expressed as [33]:

$$EC = \frac{1}{\rho}$$

Geoelectrical Measurements

A scrutiny field survey was aforethought in the study area to allocate the VES taking into consideration the availability of boreholes in order to correlate the resistivity data. In this respect, 20 VES were carried out in the study area using the Schlumberger configuration (Figure 1), with a maximum current electrode half-spacing (AB/2) of 1000m. Moreover, the digital signal enhancement resistivity meter (ABEM-TERRAMETER, SAS 4000) was used to conduct VES. Noteworthy, to ensure the interpretation accuracy, the resistivity data were measured every sixth of a logarithmic decade. On the other hand, a number of aquifer tests along with water quality sampling were employed to recognize some of the hydraulic parameters and/or hydro-chemical composition of the fresh to brackish water aquifer.

1D Geoelectric Data Inversion

In the study area, each VES was subjected to one-dimension (1D) inverse modelling, in which the iterative procedure of Zohdy [57] was applied. Iterations were carried out to reach the best fit between the smoothed field curve and the calculated one. Nevertheless, the maximum root mean square (RMS) errors of the resulting models were 5%. Noteworthy, Figure 3 displays the correlation between the interpreted resistivity layers of VES 15 and its corresponding borehole data in the area. The interpreted VES stations were used to produce two geoelectric cross-sections (profiles 1 & 2) in the study area (Figure 4). Moreover, geological subsurface data along with borehole data in the study area were integrated in this geoelectric cross-section as well. Notable, a total of four geoelectrical layers were recognized in the cross-sections (Figure 4), from top to bottom as follows:

1. A thin surficial layer characterized by true resistivity values range from 283 to 682 ohm.m. These values correspond to wadi deposits with miscellaneous nature of alluvial dry Quaternary sediments (surficial deposits of silt, sand, and gravel igneous boulders). Because of the high variation in the grain size distribution across the area (in terms of vertical and horizontal distributions), along with the spatial variation in the ratio of gravel/sand/silt, high fluctuation of the resistivity values was imputed. The thickness of this layer range between 1 and 15 m.
2. The second layer characterized by true resistivity range from 172 to 287 Ohm.m, coincide with alluvium dry Quaternary sediments of fluctuating size of silt, sand, gravel, and fine rock fragments. The thickness of this layer varies between 15 and 55 m.
3. The third layer utilized by true resistivity range between 71 and 110 Ohm.m, correspond to fresh to brackish water bearing formation of Quaternary and Pre-Quaternary alluvial sediments of silt and gravel. The thickness of the layer varies between 55 and 90 m. Conspicuously, the shape of the aquifer was greatly influenced by the surface topography of the study area.
4. The bottom (fourth) layer characterized by very low true resistivity range from 3 to 5 Ohm.m, coincide with salt water bearing formation of Quaternary and pre-Quaternary sediments of silt, sand, and gravel intercalated with some clay pocket with limited spatial extension. Worth mentioning, the fresh water of the third layer floats over the denser, more saline deeper water of the fourth layer

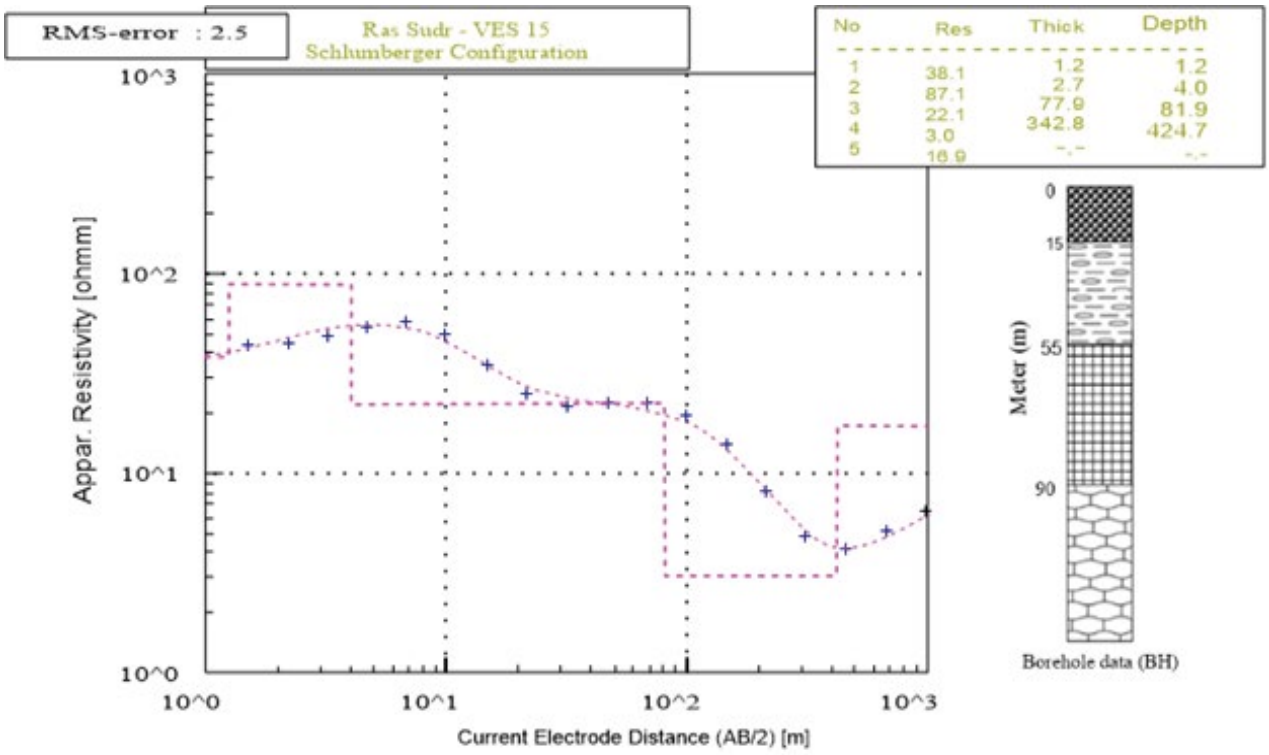

Figure 3: Correlation between the interpreted resistivity layers of VES 27 and its corresponding borehole data in the area.

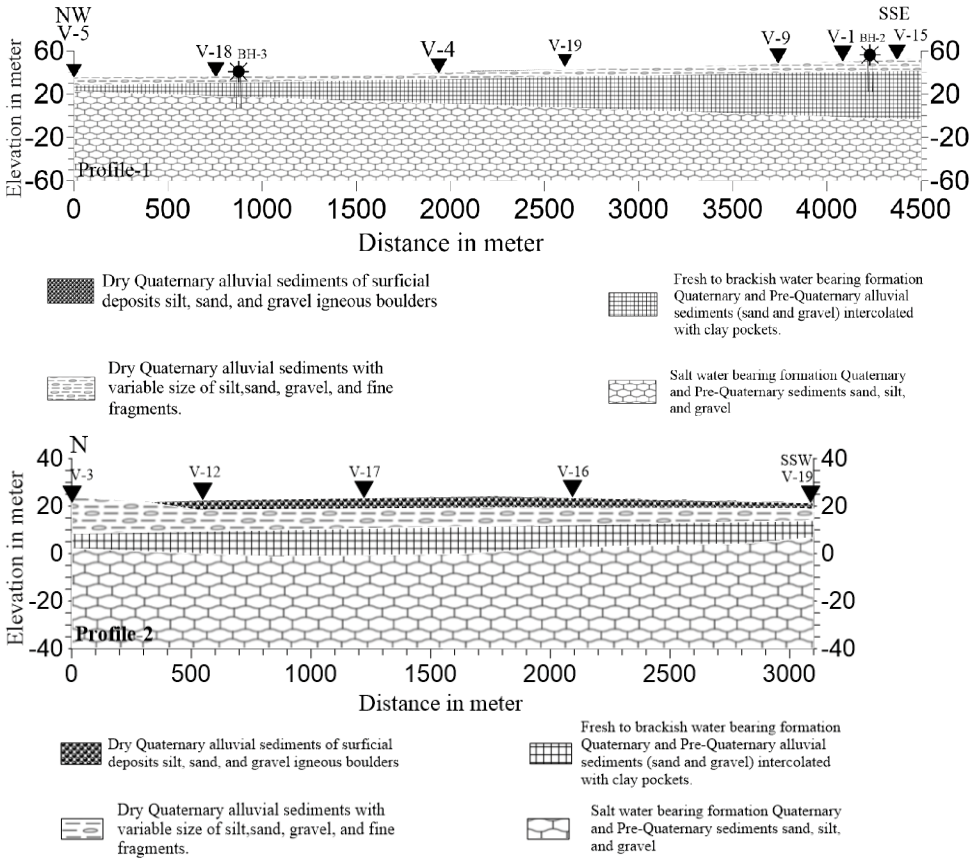

Figure 4: The geo-electric cross-sections (profiles 1 and 2) in the study area, El-Tor, Sinai. Surface elevations (m + MSL) are based on GPS with an accuracy ± 5 ~ 10 m.

Citation: Hassan NA, Khalil MH (2023) Integration of Geophysical Resistivity Inversion along with Hydrological Investigation in Scrutiny of El-Tour Coastal Aquifer. Int J Earth Sci Geophys 9:069

(Quaternary and pre-Quaternary).

Newsworthy, the fresh/saline water transition zone is effectively displayed. The highest thickness of the fresh aquifer is recognized in the eastern part of the area, especially at VES 15 (90 m) and a gradual decrease toward the western part can be observed with the lowest thickness at VES 2 (14.2 m) (Figure 5). Figure 6 illustrates a depth contour map to the top of the fresh aquifer ranged from 5 to 90 m. The minimum depth is illustrated at the

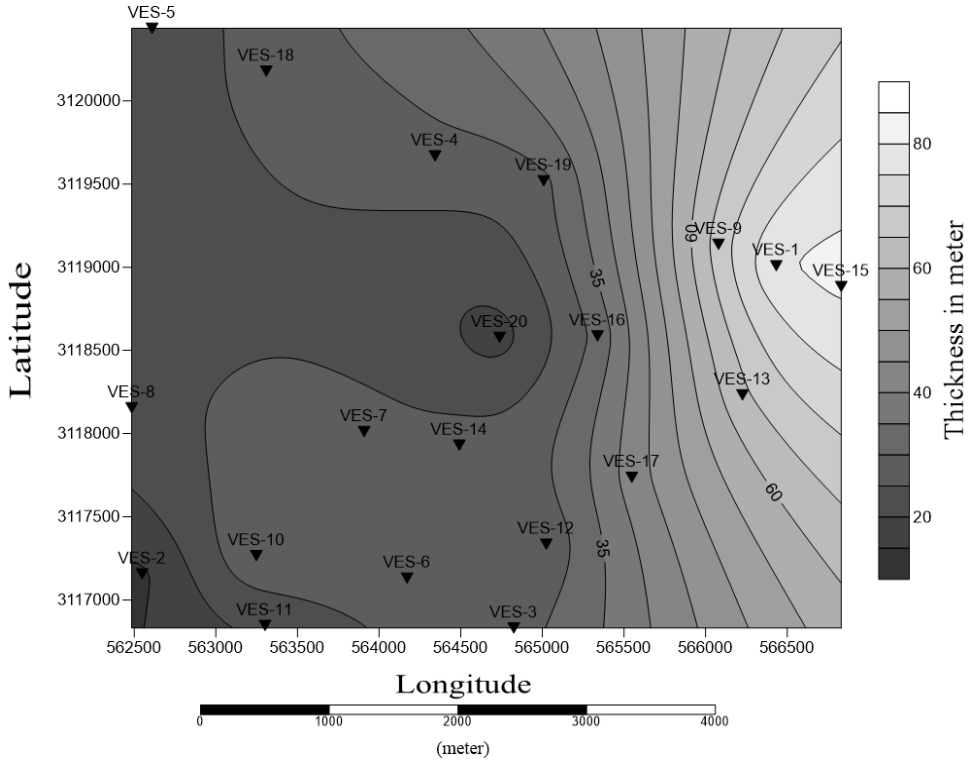

Figure 5: Thickness contour map of the fresh aquifer, El-Tor, Sinai.

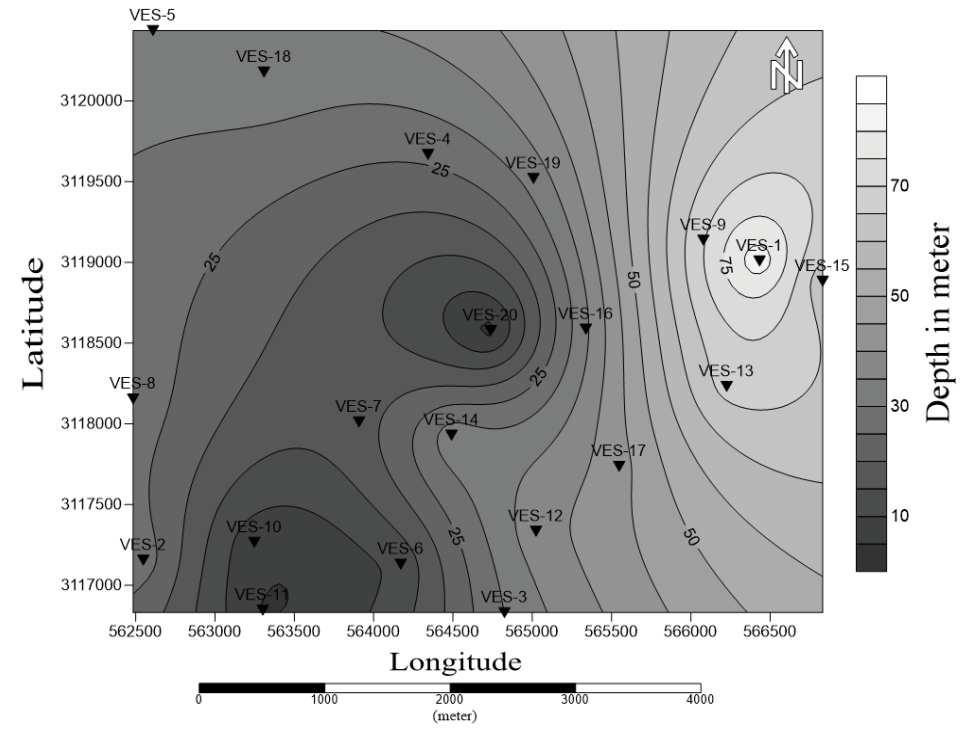

Figure 6: Depth to the top of the fresh aquifer, El-Tor, Sinai.

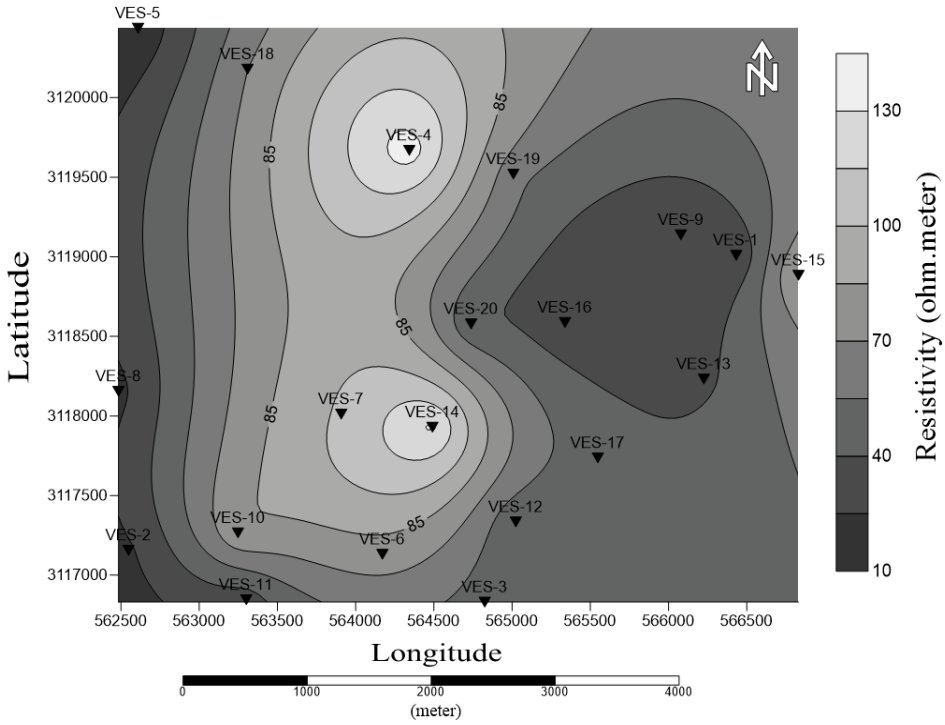

Figure 7: Resistivity contour map of the fresh aquifer, El-Tor, Sinai.

southwestern part of the area (3-18 m) with gradual increase toward the eastern zone. Moreover, the true resistivity of the aquifer ranges from 10 to 130 Ohm.m (Figure 7). Since, the geometries of the fresh aquifer indicate its sensitivity to the variation in the pumping regime, therefore, the safe yield of the fresh aquifer is controlled by its thickness.

Aquifer Hydraulic Conditions

Porosity (ϕ), tortuosity (T), hydraulic conductivity (K), transmissivity (τ), formation resistivity factor (F) as well as storativity (*S*) were investigated for the freshwater aquifer in the study area. Collins [58], pointed out, as an overarching principle the smaller the grains size, the greater the porosity (ϕ) in any natural unconsolidated material of uniform grain size [59]. In the area, porosities of the fresh water layer were obtained from the available well logs [60]. Nemours authors [61-64] stated that Tortuosity (*T*) increases with the increase of the grain size, whereas, an inverse relationship between porosity and grain size occurs. In the area, Maxwell's equation [65], was applied to calculate tortuosity from the porosity (T = (3-ϕ)/2). Abdu, et al. [66] pointed out the direct relationship between the grain size and permeability (K). Straface, et al. [67] demonstrated that various attempts have been made to establish empirical relationships between Transmissivity (τ) and different geo-electric parameters. Schopper, and Batte, et al. [68,69] emphasized that the formation resistivity factor (*F*) describing porous media is dependent on the intricate geometry of the pore channels, therefore it describes the manner in which the grains are arranged. Notable, Paterson [70], aforementioned that $F = T^2/\Phi$. In water investigations, storativity (S) has several applications such as groundwater numerical modelling, prediction of well performance, assessing the transport of contaminants, along with selection of the potential areas [71]. In the area, S were obtained from the available well logs.

In the area, the western zone is characterized by high porosity (ϕ) (42-44%) reflecting coarser grains, whereas, porosity decreases gradually toward the eastern part (37-40%) reflecting finer sediments (Table 1). For the fresh aquifer, the tortuosity ranges between 1.31 and 1.33, corresponded to an average range of porosity between 37 and 40% (Table 1). A direct relation between porosity and tortuosity can be recognized. Whereas, an inverse relation can be observed between tortuosity and grain size [72]. The pumping test of the fresh aquifer of BH-2 in the eastern zone is characterized by the highest permeability (67 m/day) (Table 1), which reflects an increase in the grain size. In the area, transmissivity values range between 1,756 and 5,432 meter^2/day

Table 1: Petro-physical hydraulic parameters of El-Tor aquifer, Sinai.

Boreholes	Porosity (ϕ) (%)	Tortuosity (*T*)	Permeability (K) (m/d)	Transmissivity (τ) (m^2/d)	Formation resistivity factor (F)	Storativity (S)
BH-1	41	1.29	56	3,565	4.06	0.227
BH-2	37	1.315	67	5,432	4.67	0.303
BH-3	44	1.28	61	1,756	3.72	0.224

(Table 1). The highest transmissivity is observed at BH-2, which indicates high yielding potentiality of the aquifer in this sector. Paterson [70], equation is used to calculate the formation resistivity factor which range between 3.72 and 4.67 (Table 1). BH-2is characterized by the highest formation factor (4.67) which reflect higher aquifer potentiality and better characteristics [73]. Storativity (S) of the Quaternary aquifer is deduced from the pumping test and range from 0.224 (BH-3) to 0.303 (BH-2) (Table 1). Should be acknowledge, these results are in good agreement with the typical value corresponding to unconfined aquifer with shallow depths [74].

Aquifer Electrical Conditions

In the area, electric anisotropy (λ) along with electric conductivity (EC) were analyzed for the fresh aquifer.

A) Electric anisotropy (λ)

In the study area, the above mentioned Dar-Zarouk geo-electric parameters were reckoned to the top of the fourth layer of the saline water bearing formation. The total longitudinal conductance (S_t) range between 0.21 and 3.58 1/Ohm. The maximum total conductance (S_t) is revealed at VES-15 and the minimum at VES-14 (Figure 8a). Oteri [75], pointed out that the remarkable increase in S_t may concur with an average increase in the clay content. The total transverse resistance (T_t) range from 727 to 18266 Ohm.m^2. Noteworthy, the maximum T_t value is recorded at VES-7 and the minimum at VES-20 (Figure 8b). The average longitudinal resistivity (ρ_l) range between 9.1 and 158 Ohm.m. The minimum ρ_l is observed at VES-2 while the maximum is displayed at VES-14 (Figure 8c). The average transverse resistivity (ρ_t) range between 24 and 507 Ohm.m. The minimum ρ_t is observed at VES-15, whereas the maximum is recorded at VES-7 (Figure 8d). Noteworthy, ρ_t is generally greater than ρ_l which indicate that the average hydraulic conductivities and current flow along the bedding planes are greater than those normal to the bedding planes [76]. According to Keller [77], ρ_l is governed by the more conductive layers, whereas ρ_t rapidly increase even if a small fraction of resistive layers were present. The prior clarification introduced the concept of electric anisotropy (λ) in the area which range from 1 to 2.1. The minimum (λ) is observed at VES-15 and the maximum is revealed at VES-10 (Figure 8e). On the other hand, the isotropic layers alternation can be transmuted into an equivalent heterogeneous and anisotropic structure. Pursuant to Rucker, et al. [78] this anisotropy may interpret as a result of alternating layers of clay and fine sands and/or the intercalation of different grain sizes in the same layer. However, in the area, anisotropy can be due to both of these two conditions. Noteworthy, the eastern sector of the area is characterized by low values of anisotropy which corresponded to high aquifer potential zones [79]. The mean resistivity (ρ_m) ranges from 17 to 244 Ohm.m. The minimum ρ_m is observed at VES-5 and the maximum is at VES-7 (Figure 8f). The change of the resistivity is dependent upon the direction of flow and the influence of lithology variation when there is a difference between the longitudinal, transverse, and mean resistivities.

B) Electrical conductivity (EC)

EC was measured for layers 3 and 4 corresponded to the fresh and saline aquifer, respectively (Table 2). Solinst TLC conductivity meter (Model 107) was used for EC measurements. The smart conductivity probe demonstrates conductivity that has been standardized to 25 °C, i.e., specific conductance, providing standardized repeatable comparable measurements. Furthermore, the Solinst TLC meter provides simple and proper calibration either by single-or double-point calibration. The measurements were carried out downward with a 1 m interval. EC measurements in the area range from 0.017 to 0.048

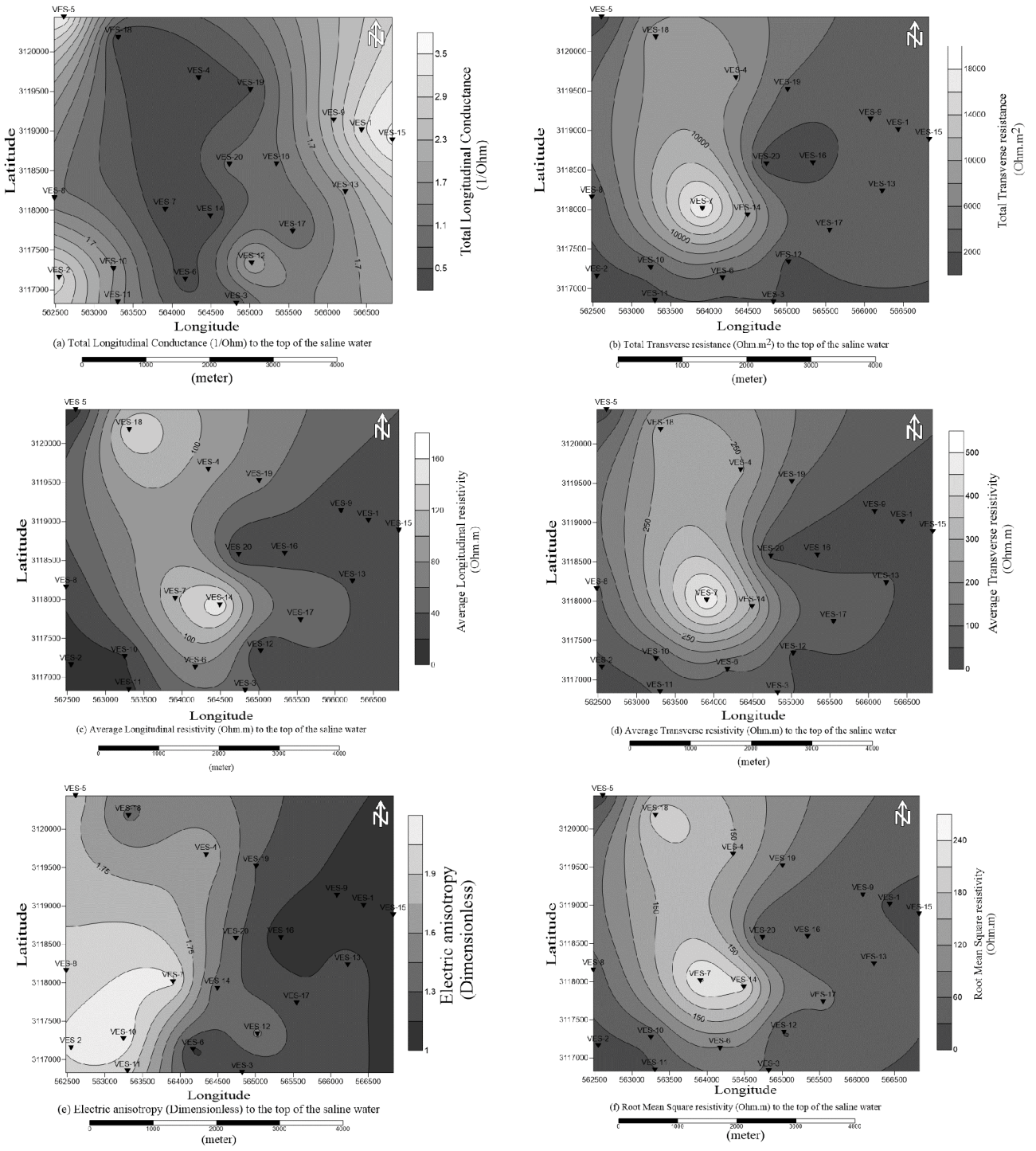

Figure 8: Geo-electric (Dar-Zarouk) parameters to the top of the saline aquifer, El-Tor, Sinai.

Table 2: Electric conductivity of El-Tor aquifer, Sinai.

Borehole locations	Electric conductivity (mS/m)
BH-1	0.025 to 0.193
BH-2	0.048 to 0.356
BH-3	0.017 to 0.562

mS/m for the fresh aquifer, while range from 0.193 to 0.562 mS/m for the saline aquifer.

Pumping Regime and Aquifer Loss (M)

Well test was conducted to predict the maximum rate at which water can be pumped from a well along with water fall level (drawdown) for a given pumping rate. Furthermore, total drawdown in a well (St) can be manifested using Meier, et al. [80] equation, were:

St = Sa + Sw

Sa: Drawdown in the aquifer at the radius of the

pumping well (aquifer loss).

Sw: Drawdown inside the well (well loss).

Due to the aquifer laminar flow resistance, aquifer loss (m) is instigated and is usually independent of the pumping rate. On the other hand, the specific capacity (m^2/h) illustrates the well yield per unit of drawdown [81]. Of the most significant consideration in well design is well efficiency (E) as well as in well construction and development. Jacob [82], defined well efficiency (E) as; E = (Sa/St) × 100. Worth mentioning, the well yield depends on the aquifer characteristics, well parameters and the pump efficiency [83]. In the study area, well loss (m), aquifer loss (m), specific capacity (m^2/h), and efficiency (%) were carried out for BH-2 and BH-3 with different pumping rates (m^3/day). Ground Water for Windows package (GWW) was used to evaluate the acquired data of the step-drawdown test [84]. Figure 9 displays graphically the analyses results. To be noticed, an increase in the pumping rate was accompanied by an increase in both well and aquifer losses along with a decrease in well specific capacity and well efficiency. Therefore, for each development well, the pumping rate must be optimized to obtain the highest well efficiency and well specific capacity with less well and aquifer losses. Consequently, an adequate well design and appropriate pumping rate are essential to maintain the aquifer, decrease well loss, and ensure a long operating life.

Aquifer Hydro-Chemical Conditions

Total dissolved solids (TDS), major cations (K, Na, Mg, and Ca), and major anions (Cl, SO_4 and HCO_3) was sampled and chemically analyzed for fresh aquifer at BH-1 to BH-3 (Table 3). To be noticed, BH-2isutilized by the lowest TDS concentrations of 496 ppm indicating freshwater along with NaCl-$CaSO_4$ ionic type and Na_2SO_4 and $MgCl_2$ genetic types. Moreover, BH-2 is located in the middle of the El-Qaa plain and mainly recharged by wadis of the eastern mountainous of the Pre-Cambrian crystalline basement. Accordingly, it receives higher amounts of recharge. Furthermore, BH-2 is characterized by high hydraulic conductivity of 52 m/day (Table 3) causing higher flow velocity and good conditions for water desalination. BH-3 is utilized by TDS concentrations of 1,679 ppm indicated brackish water. BH-3 has NaCl-$CaSO_4$ ionic type and Na_2SO_4 and $MgCl_2$ genetic types. Based on the hydro-chemical parameters (Table 3), the best water quality can be recognized in the eastern part at BH-2 and the worst toward the western

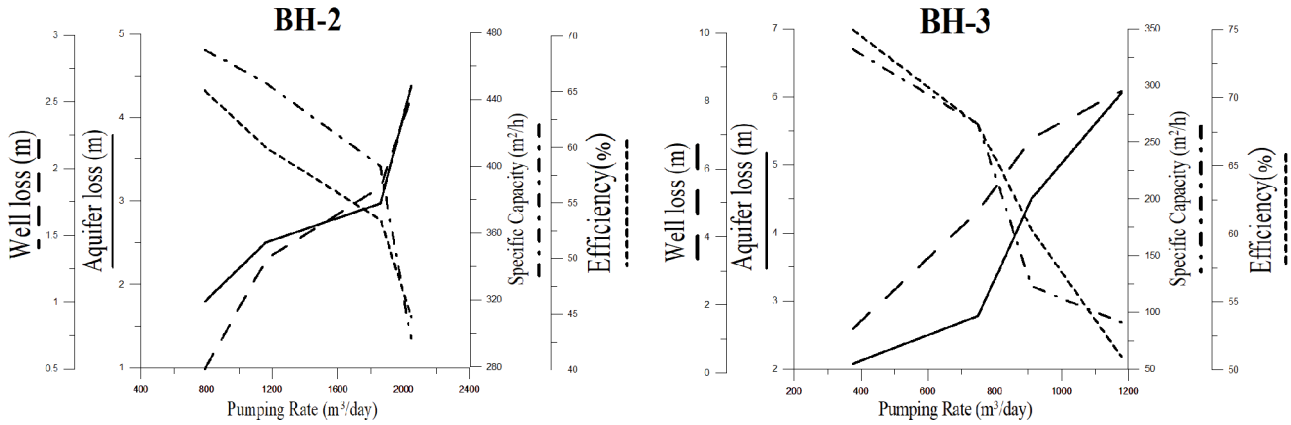

Figure 9: Well hydraulic parameters of BH-2 and BH-3, El-Tor, Sinai.

Table 3: Collected water samples and the corresponding average concentrations (ppm) of TDS, Na, Mg, Ca, Cl, SO_4, and HCO_3 for the fresh aquifer, El-Tor, Sinai.

Locations (VES and Boreholes)	TDS	K	Na	Mg	Ca	Cl	SO_4	HCO_3
BH-1	1,137	3.21	319.2	16.9	86.8	556.7	87.2	52.2
BH-2	496	2.13	107.4	9.48	52.3	195.5	85.66	37.1
BH-3	1,679	5.0	445.4	23.1	128.9	845.5	129.2	74.5

part at BH-3. The good correlation between SO_4 and Cl pointed to the mixing processes between different water geneses. Davis and De Wiest [85], pointed out that the good correlation between ionic concentrations of HCO_3 and K referred to the release of K cations from rock material by the percolated meteoric water. Therefore, a network of monitoring wells is highly recommended to observe the changes in the groundwater quality and protect the aquifer from deterioration.

Conclusion

Scouting of the freshwater qualitative and quantitative conditions in the El-TOR coastal aquifer was carried out through integrating 1D Schlumberger geoelectric resistivity inversion, along with geohydrologic analysis, borehole data, pumping tests and hydro-chemical analysis. On top of that, a number of electric and hydraulic conditions were investigated. A total of 20 VES with a maximum AB/2 of 1000 m were conducted in the area. The results demarcate effectively the fresh aquifer with thickness and true resistivity range from 55 to 90 m and 71 to 110 Ohm.m, respectively (Figure 5 and Figure 7). Furthermore, a notable potential of the freshwater aquifer is recognized toward the eastern zone of the area with a maximum aquifer thickness of 90m. Praiseworthy, freshwater aquifer is characterized by porosity of 37%, tortuosity of 1.31, and permeability of 56 m/day. In addition to, transmissivity, formation resistivity factor, and Storativity of 3,565 m^2/day, 4.67 and 0.224, respectively (Table 1). Not only, the eastern sectoris characterized by increased values of electrical conductivity (0.048 to 0.356), but also with low values of TDS (496 ppm) (Table 2 and Table 3) demonstrating coarser grains size along with high groundwater yielding potentiality. The average transverse resistivity (ρ_t) is generally greater than the average longitudinal resistivity (ρ_l) which indicated that the average hydraulic conductivities and current flow along the bedding planes were greater than those normal to the bedding planes [86]. Moreover, ρ_l was governed by the more conductive layers, whereas ρ_t rapidly increased even if a small fraction of resistive layers were present. In the area, electric anisotropy (λ) range from 1 to 2.5 (Figure 8), whereas, the mean resistivity ranges from 17 to 255 Ohm.m. Electrical conductivity for the fresh aquifer (third layer) range from 0.015 to 0.045 mS/m, while range from 0.208 to 0.769 mS/m for the saline aquifer (fourth layer). Figure 9 illustrate the well loss (m), aquifer loss (m), well specific capacity (m^2/h), and well efficiency (%) employed for BH-1 and BH-3 with different pumping rates (m^3/day). Noteworthy, an increase in the pumping rate is accompanied by an increase in both well and aquifer losses, as well as decreasing in the well specific capacity and well efficiency (Figure 9). Consequently, an adequate well design and appropriate pumping rate are essential to maintain the aquifer, decrease well loss, and ensure a long operating life.

References

1. SEAM Programme (1999) South Sinai environmental and development profile. Egyptian Environmental Affairs Agency, 28.
2. Quick Bird, March, 2010 and the datum for geographic coordinates is WGS-1984.
3. Rushdi S (1990) Geology of Egypt. Balkema, Rotterdam, 722.
4. Sultan AS, Mahmoud IM, Fernando MS (2009) Hydrogeophysical study of the El Qaa Plain, Sinai, Egypt. Bulletin of Engineering Geology and the Environment 68: 525-537.
5. Shata AMM, El Shazli MS, Diab TA, Abdel L, Tamer MA (1992) Preliminary report on the groundwater resources in the Sinai Peninsula, Egypt, parts I and II. The Desert Institute, Water Resources Department, Cairo, 92-105.
6. Abdel Moneim AA (2005) Overview of the geomorphological and hydrogeological characteristics of the Eastern Desert of Egypt. Hydrogeology Journal 13: 416-425.
7. Khalil MH (2006) Geoelectric resistivity sounding for delineating salt water intrusion in the Abu Zenima area, west Sinai, Egypt. Journal of Geophysics and Engineering 3: 243-251.
8. Khalil MH, Hanafy SM, Gamal MA (2008) Preliminary seismic hazard assessment, shallow seismic refraction and resistivity sounding studies for future urban planning at Gebel Umm Baraqa area, Egypt. Journal of Geophysics and Engineering 5: 371-386.
9. Khalil MH (2010) Hydro-geophysical Configuration for the Quaternary Aquifer of Nuweiba Alluvial Fan. Journal of Environmental and Engineering Geophysics (JEEG) 15: 77-90.
10. Ahmed M, Sauck W, Sultan M, Yan E, Soliman F, et al. (2014) Geophysical Constraints on the Hydrogeologic and Structural Settings of the Gulf of Suez Rift-Related Basins: Case Study from the El Qaa Plain, Sinai, Egypt. Surveys in Geophysics 35: 415-430.

11. El-Fadl MMA, M El-Aassar A-H M, Khaled MA (2018) Assessment of water resources setting using hydrogeochemistry and geophysic study El-Tur area, South Sinai Governorate, Egypt. Environmental Science 5: 187-203.

12. (1999) The authority of the geological survey of Egypt.

13. Shendy EH (1984) Geological and geophysical investigation for groundwater in El-Qaa plain, Southwestern Sinai. MSc thesis, Faculty of Science, Suez Canal University, Ismalia, Egypt.

14. Wannous M, Jahnke C, Troeger U, Troeger U, Falk M (2021) Hydrochemistry and environmental isotopes (^{18}O, ^{2}H, ^{3}H, $^{3}He/^{4}He$) of groundwater and floodwater in the great area of Hurghada, Eastern Desert of Egypt. Environmental Earth Science 80: 407.

15. Khalil MH (2012) Magnetic, geo-electric, and groundwater and soil quality analysis over a landfill from a lead smelter, Cairo, Egypt. Journal of Applied Geophysics 86: 146-159.

16. Jahnke C, Wannous M, Troeger U, Falk M, Struck U (2019) Impact of seawater intrusion and disposal of desalinization brines on groundwater quality in El Gouna, Egypt, Red Sea Area, Process analyses by means of chemical and isotopic signatures. Applied Geochemistry 100: 64-76.

17. Khalil MH (2009) Hydrogeophysical assessment of Wadi El-Sheikh aquifer, Saint Katherine, South Sinai, Egypt. Journal of Environmental and Engineering Geophysics (JEEG) 14: 77-86.

18. Leppard CW, Gawthorpe RL (2006) Sedimentology of rift climax deep water systems; Lower Rudeis formation, Hammam Faraun Fault Block, Suez Rift, Egypt. Sedimentary Geology 191: 67-87.

19. Webster DI, Riston N (1982) Post- Eocene stratigraphy of the Suez rift in south-west Sinai, Egypt. E.G.P.C. Sixth Exploration Seminar, Cairo, Egypt 1: 276-288.

20. Rizkalla RI (1985) Preliminary statistical gravimetric tectonic trend analysis in Sinai Peninsula and its surroundings, Egypt. 10th International Congress for Statistics, Computer Science, Social and Democratic Research.

21. Dames, Moore (1985) Sinai development study, phase 1, final report. water supplies and coast. The Advisory Committee for Reconstruction Ministry of Development, Arab Republic of Egypt, 5.

22. Meshref WM, El-Kattan MI (1989) Tectonic pattern of El-Qaa plain, Sinai using Aeromagnetic data. 2nd conference, Geology of Sinai for Development, Ismailia, 33-42.

23. Gorski J, Ghodeif K (2000) Salinization of shallow water aquifer in El-Qaa coastal plain, Sinai, Egypt. Proceedings of 16th salt water intrusion meeting, Wolin Island, Poland.

24. Abd El Samie S, Sadek M (2001) Groundwater recharge and flow in the Lower Cretaceous Nubian Sandstone aquifer in the Sinai Peninsula, using isotopic techniques and hydrochemistry. Hydrogeology Journal 9: 378-389.

25. Sayed MAA, El-Fakharany MA, Hamed MF (2004) Integrated geophysical and hydrogeological studies on the Quaternary aquifer at the middle part of El-Qaa plain, SW Sinai, Egypt. Egyptian Geophysical Society, EGS Journal 2: 135-145.

26. Usama M, Fernando S, Gad E-Q, Magdy A, Mamdouh S (2009) Identification of the shallow subsurface succession and investigation of the seawater invasion to the Quaternary aquifer at the northern part of El Qaa plain, Southern Sinai, Egypt by transient electromagnetic data. Geophysical Prospecting 58: 267-277.

27. Abo El-Fadl Moustafa M, Abdel-Hameed M El-Aassar, Khaled MA (2018) Assessment of water resources setting using hydrogeochemistry and geophysic study El-Tur area, South Sinai Governorate, Egypt. Journal of Basic and Environmental Sciences 5: 187-203.

28. Muhammad H, Yanjun S, Weijun J, Gulraiz A (2021) Estimation of hydraulic parameters in a hard rock aquifer using integrated surface geoelectrical method and pumping test data in southeast Guangdong, China. Geoscience Journal 25: 223-242.

29. Shakeel A, de Marsily Ghislain, Alain T (1988) Combined use of hydraulic and electrical properties of an aquifer in a geostatistical estimation of transmissivity. Ground Water 26: 78-86.

30. Benson AK, Payne KL, Stubben MA (1997) Mapping groundwater contamination using DC resistivity and VLF geophysical methods - A case study. Geophysics 62: 80-86.

31. Nassir SSA, Loke MH, Lee CY, Nawawi MNM (2000) Salt-water intrusion mapping by geo-electrical imaging surveys. Geophysical Prospecting 48: 647-661.

32. Louis IF, Karantonis GA, Voulgaris NS, Louis FI (2004) The contribution of geophysical methods in the determination of aquifer parameters: The case of Mornos River delta, Greece. Journal of Chemistry and Environment 8: 41-49.

33. Atekwana Eliot A, Atekwana Estella A, Rowe Rebecca

S, Werkema Jr D Dale, Legall Franklyn D (2004) The relationship of total dissolved solids measurements to bulk electrical conductivity in an aquifer contaminated with hydrocarbon. Journal of Applied Geophysics 56: 281-294.

34. Apostolopoulos G (2008) Combined Schlumberger and dipole-dipole array for hydro geologic applications. Geophysics 73: F189-F195.

35. Abdel Aal GZ, Atekwana EA, Rossbach S, Werkema DD (2010) Sensitivity of geo-electrical measurements to the presence of bacteria in porous media. Journal of Geophysical Research 115.

36. Khalil MH, Hassan NA (2016) Ground magnetic, GPR, and dipole-dipole resistivity for landfill investigation. International Journal of Geoscience 7: 828-848.

37. Lashkaripour GR, Ghafoori M, Dehghani A (2005) Electrical resistivity survey for predicting Samsor aquifer properties, southeast Iran. Geophysical Research Abstracts 7.

38. Niwas S, Singhal DC (1981) Estimation of aquifer transmissivity from Dar Zarrouk parameters in porous media. Hydrology 50: 393-399.

39. Onuoha KM, Mbazi FCC (1988) Aquifer transmissivity from electrical sounding data: The case of Ajali sandstone aquifers South-west of Enugu, Nigeria. Ground Water and Mineral Resources of Nigeria, Vieweg Verlag, 17-30.

40. Mazac O, Cislirova M, Kelly WE, Landa I, Venhodova D (1990) Determination of hydraulic conductivities by surface geoelectrical methods. Society of Exploration Geophysics 125-131.

41. Mbonu PDC, Ebinero JO, Ofoegbu CO, Ekine AS (1991) Geoelectric sounding for the determination of aquifer characteristics in parts of the Unuahia area of Nigeria. Geophysics 56: 284-192.

42. Asfahani J (2006) Neogene aquifer properties specified through the interpretation of electrical sounding data, Salamiyeh region, central Syria. Hydrological Processes 21: 2934-2943.

43. Ghaib Fadhil A (2009) The assessment of Erbil aquifer using geo-electrical investigation (Iraqi Kurdistan Region). Journal of Applied Sciences in Environmental Sanitation 4: 43-54.

44. Marsden D (1973) The automatic fitting of a resistivity sounding by a geometrical progression of depth. Geophysical Prospecting 21: 266-280.

45. Moench AF, Garabedian SP, Le Blanc DR (2001) Estimation of hydraulic parameters from an unconfined aquifer test conducted in a glacial outwash deposit, Cape Cod, Massachusetts. U.S. Geological Survey.

46. Banerjee KS, Sharma SP, Sarangi AK, Sengupta D (2011) Delineation of subsurface structures using resistivity, VLF, and radiometric measurement around a U-tailings pond and its hydrogeological implication. Physics and Chemistry of the Earth, Parts A/B/C 36: 1345-1352.

47. Bobachev C (2002) IPI2Win: A Windows software for an automatic interpretation of resistivity sounding data. PhD Thesis, Moscow State University, Russia.

48. Batte G, Muwang A, Sigrist WP (2008) Evaluating the use of vertical electrical sounding as a groundwater exploration technique to improve on the certainty of borehole yield in Kamuli district (Eastern Uganda). African Journal of Science and Technology 9: 72-85.

49. Zohdy AAR, Eaton GP, Mabey DR (1974) Application of surface geophysics to groundwater investigations, techniques of water resources investigation, U.S. Geological Survey, Techniques of Water-Resources Investigations, Washington, 116.

50. Worthington PF (1976) Quantitative geophysical investigations of granular aquifers. Geophysics Survey 2: 313-366.

51. Campbell DL (1977) Model for estimating electric macro anisotropy coefficient of aquifers with horizontal and vertical fractures. Geophysics 42: 114-117.

52. Cardiff M, Barrash W, Kitanidis PK (2013) Hydraulic conductivity imaging from 3-D transient hydraulic tomography at several pumping/observation densities. Water Resources Research 49: 7311-7326.

53. Hasan M, Shang Y, Jin W, Akhter G (2019d) Investigation of fractured rock aquifer in South China using electrical resistivity tomography and self-potential methods. Journal of Mountain Science 16: 850-869.

54. Maillet R (1947) The fundamental equations of electrical prospecting. Geophysics 12: 529-556.

55. Majumdar RK, Das D (2011) Hydrological characterization and estimation of aquifer properties from electrical sounding data in Sagar Island region, South 24 Parganas, West Bengal, India. Asian Journal of Earth Sciences 4: 60-74.

56. Nasser M, Lee S (2007) Aquatic electrical resistivity imaging of shallow-water wetlands. Geophysics 72: F211-F221.

57. Zohdy AAR (1989) A new method for automatic

interpretation of Schlumberger and Wenner sounding curves. Geophysics 54: 245-253.

58. Collins RE (1961) Flows of fluids through porous materials. Reinhold Chemical Engineering Series, Reinhold Publishing Corporation, New York, 270.

59. Kofi BF, Seabrook, Brian (2000) Estimating hydraulic conductivity and porosity of soils from spectral electrical response measurements. Journal of Environmental and Engineering Geophysics 5: 1-9.

60. (2001) Desert Research Institute (DRI) - Petro-physical Parameters and Well Logging Department, Cairo, Egypt.

61. Wyllie MRJ, Gregory AR (1953) Formation factors of unconsolidated porous media: Influence of particle shape and effect of cementation. Journal of Petroleum Technology 198: 103-104.

62. Perkins FM, Osoba JS, Ribe KH (1956) Resistivity of sandstone as related to the geometry of their interstitial water. Geophysics 21: 1071-1086.

63. Corey AT (1977) Mechanics of heterogeneous fluids in porous media. Water Resources Publications, Colorado, 259.

64. Attwa M, Basokur A, Akca I (2014) Hydraulic conductivity estimation using direct current (DC) sounding data: a case study in East Nile Delta Egypt. Hydrogeology Journal 22: 1163-1178.

65. Maxwell JCA (1881) Treatise on electricity and magnetism. Oxford University Press, United Kingdom.

66. Abdu H, Robinson DA, Seyfried M, Jones SB (2008) Geophysical imaging of watershed subsurface patterns and prediction of soil texture and water holding capacity. Water Resources Research 44.

67. Salvatore S, Enzo R, Francesco C (2010) Estimation of hydraulic conductivity and water table map in a large-scale laboratory model by means of the self-potential method. Journal of Geophysical Research 115: B06105.

68. Schopper JR (1966) A theoretical investigation on the formation factor/permeability/porosity relationship using a network model. Geophysical Prospecting 14: 301-341.

69. Batte AG, Barifaijo E, Kiberu JM, Kawule W, Muwanga A, et al. (2010) Correlation of geoelectric data with aquifer parameters to delineate the groundwater potential of hard rock terrain in Central Uganda. Pure Applied Geophysics 167: 1549-1559.

70. Paterson MS (1983) The equivalent channel model for permeability and resistivity in fluid-saturated rock - A pre-appraisal. Mechanics of Materials 2: 345-352.

71. Glaser Danney R, Fink James B, St Louis Robert M, Bell Ronald S (2009) High resolution resistivity mapping of subsurface controls on acid rock drainage at an active mine site. Symposium on the Application of Geophysics to Engineering and Environmental Problems conference.

72. Claude D, Ruy Stephane (2010) Prediction of unsaturated soil hydraulic conductivity with electrical conductivity. Water Resources Research 45: W10408.

73. Hassan Noha A, Khalil MH, Mahmoud G (2020) Magnetic and geo-electrical geophysical techniques for subsurface delineation and groundwater assessment in Ras Matarma, Sinai. Journal of Environmental and Engineering Geophysics 25: 425.

74. Mishra PK, Neuman SP (2011) Saturated-unsaturated flow to a well with storage in a compressible unconfined aquifer. Water Resources Research 47: W05553.

75. Oteri AU (1981) Geoelectric investigation of saline contamination of chalk aquifer by mine drainage water at Tilmanstone, England. Geoexploration 19: 179-192.

76. Niwas S, de Lima OAL (2003) Aquifer parameter estimation from surface resistivity data. Groundwater 41: 94-99.

77. Keller GV (1982) Electrical properties of rocks and minerals. In: Carmichael RS, Handbook of Physical Properties of Rock, CRC Press, 217-293.

78. Rucker DF, Noonan GE, Greenwood WJ (2011) Electrical resistivity in support of geological mapping along the Panama Canal. Engineering Geology 117: 121-133.

79. Singh CL, Singh SN (1970) Some geoelectrical investigations for potential groundwater in part of Azamgrah area of U.P. Pure and Applied Geophysics 82: 270-285.

80. Meier PM, Carrera J, Sanchez-Vila X (1998) An evaluation of Jacob's method for the interpretation of pumping tests in heterogeneous formations. Water Resources Research 34: 1011-1025.

81. Meier PM, Medina A, Carrera J (2001) Geostatistical inversion of cross-hole pumping tests for identifying preferential flow channels within a shear zone. Ground Water 39: 10-17.

82. Jacob CE (1947) Drawdown test to determine effective radius of artesian well. Transactions of the American Society of Civil Engineers 112: 1047-1070.

83. Niemann WL, Rovey CW II (2007) Comparison

of hydraulic conductivity values obtained from aquifer pumping tests and conservative tracer tests. Groundwater Monitoring & Remediation 20: 122-128.

84. Braticevic D, Karanjac J (1997) Ground Water for Windows (version 1.31) software and manual. Department for Development Support and Management Services, United Nation.

85. Davis SN, De Wiest RJM (1966) Hydrogeology. John Wiley & Sons, New York, 463.

86. Flathe H (1955) Possibilities and limitations in applying geoelectrical methods to hydrogeological problems in the coastal area of northwest Germany. Geophysical Prospecting 3: 95-110.

DOI: 10.35840/2631-5033/1869

Citation: Hassan NA, Khalil MH (2023) Integration of Geophysical Resistivity Inversion along with Hydrological Investigation in Scrutiny of El-Tour Coastal Aquifer. Int J Earth Sci Geophys 9:069